Synthesis and molecular docking study of new thiazolidinones incorporating a benzoate moiety as anti-HepG2 cancer agents, EGFR inhibitors and apoptosis inducers

Salwa Magdy Eldaly
Cairo University-Giza
Dalia Salama Zakaria
Cairo University-Giza
Nadia Hanafy Metwally (mnadia@sci.cu.edu.eg)
Cairo University-Giza

Research Article

Keywords: Thiazolidinones, EGFR protein kinase, cell cycle DNA-flow cytometric, Annexin V-FITC

Posted Date: January 10th, 2023

DOI: https://doi.org/10.21203/rs.3.rs-2444022/v1

Abstract

Synthesis of new anticancer candidates with protein kinases inhibitory potency is a major goal of pharmaceutical science and synthetic research. This current work represents the synthesis of a series of substituted thiazolidinones incorporating a benzoate moiety, starting from 4-formylphenyl benzoate **1a** and 4-formyl-2-methoxyphenyl benzoate **1b**. Most prepared thiazolidinones **5a-j**, **7a-h** and **9a-j**, were evaluated *in vitro* for their potential anticancer activity against three cell lines (HepG2, MCF-7 and HeLa). The most active cytotoxic compounds **3a**, **3b**, **5a**, **5c** and **5h** were then further tested against the normal cell line WI38. All of these were shown be more effective toward anticancer cell lines. Thiazolidinones **5c** and **5h** were further evaluated to be kinase inhibitors against EGFR showing effective inhibitory impact. Furthermore, **5c** and **5h** were tested for their effects on cell cycle and apoptosis induction capability in HepG2 cell lines by DNA-flow cytometry analysis and annexin V-FITC apoptosis assay, respectively. The results showed that they have effect of disrupting the cell cycle and causing cell mortality by apoptosis in the treated cells. Moreover, molecular docking studies by the Moe 2015 program showed better binding patterns for **5c** and **5h**with the active site of the EGFR protein kinase [PDB code 1M17]. Finally, toxicity risk and physicochemical characterization was performed for most of the compounds, revealing excellent properties as possible drugs, especially compounds **5c** and **5h**.

1. Introduction

Cancer is a major problem affecting people`s lives worldwide, threatening both developed and developing countries and causing high ratio in death incidence. [1] Its incidence is reported to reach about 29.5 million cases each year in 2040. [2, 3] Liver cancer ranks sixth in the world among all malignancies. It's considered the third most deadly cancer type among all. [4] It is estimated that by 2025, more than 1 million people will be diagnosed with liver cancer annually. [5] Hepatocellular carcinoma (HCC) is the most occurring type of liver cancer and causing about 90% of cases. Unfortunately, chemotherapeutic agents used to treat cancer are not selectivity other than their toxicity and resistance. [6] Therefore, extensive efforts has been devoted to developing new drugs that target only cancer cells. [7] Current drug discovery research targets protein kinases [8], which play critical role in cell proliferation and mobility so any dysfunctions occurred because of kinases mutations lead to cellular abnormalities and successively developing of cancer initiation, progression or even metastasis. [9] As such, protein kinases are considered as drug targets for chemotherapeutic agents, one of which is EGFR. [10–12]

Epidermal growth factor receptor (EGFR) is a trans-membrane glycoprotein that belong to the category of receptor tyrosine kinases and plays a key role in cell signaling pathways including cell proliferation, apoptosis, angiogenesis and metastatic invasion. [13] High-levels of his EGFR due to its overexpression are found in many types of human cancers, such as hepatocellular carcinoma and brain cancer, so EGFR is a remarkable target in the treatment of different types of cancer. [14–18] Late-stage of hepatocellular carcinoma shows, increased EGFR abundance that leads to increased proliferation and tumor differentiation. [19, 20] Recent studies on EGFR inhibitors in human hepatocellular carcinoma cell lines have enhanced our understanding of EGFR signaling mechanism in hepatocellular carcinoma and thus will improve the application of these inhibitors in liver cancer therapy. [21–25] The EGFR pathway is inactivated by tyrosine kinase inhibitors (TKIs) like Gefitinib and Erlotinib (Fig. 1). They are antagonists of binding to the EGFR adenosine triphosphate pocket, in turn inactivating EGFR auto-phosphorylation and downstream signaling. [26–29] Reportedly, resistance to cancer therapy arising from anticancer drugs, radiotherapy and even hormonal therapy was caused by over-expression of EGFR in variety of human cancers. [30, 31] Therefor, in his case with advanced EGFR mutations, anti-EGFR drugs are the first line of treatment, as they are highly effective and safe compared to other standard chemotherapeutic drugs. [32–34] The drug design research field affirms that thiazoles and thiazolidinones are effective moieties in chemotherapeutic drugs. They participate in the construction of many significant compounds with different biological activities. [35–39] There are thiazole-containing compounds that have been reported as potent anticancer agents that target the kinases signaling pathway [40] such as Dasatinib and Dabrafenib (Fig. 1) that considered as thiazole selective drugs with tyrosine kinase inhibitory activity. [41–42] In addition there are approved drugs containing thiazolidinone core structures such as Etozoline and Ralitoline (Fig. 1). Moreover, many thiazolyl-containing compounds have been found to be potent cytotoxic agents against different cell lines. As an example, compound **I** showed potent cytotoxic activity towards mammary gland breast cancer cell line MCF-7 (acronym for Michigan Cancer Foundations-7) with IC_{50} of 0.07 μM besides being EGFR inhibitor with IC_{50} of 0.06 μM. [43, 44] Additionally, the thiazolyl-3-arylpyrazole-4-carbaldehyde **II** has a significant cytotoxic activity against the cervical epithelioid carcinoma cell line HeLa with IC_{50} of 5.75 μM. [45] Also, Channar *et al.* have designed and synthesized thiazolidinone **III** with excellent cytotoxic activity in MCF-7 and HeLa cell lines. [46] Furthermore, the indole-thiazolidinone **IV** revealed cytotoxic activity in MCF-7, colon cancer HCT116 and lung cancer A549. [47] Besides, the thiazolone-pyrazoles **V-VI** represented potent EGFR inhibition capability. [48] In addition, the arylidene derivatives of thiazolidinone **VIIa-c** showed cytotoxic activity in MCF-7 and hepatocellular carcinoma HepG2. [49] It was alsorecently reported that thiazolidinone **VIII** exhibited antiproliferative activity targeting HepG2, MCF-7 and HCT116 cell lines (Fig. 2). [50]

Taking into account the aforementioned data and as an extension of our ongoing research work on the designing biologically active heterocyclic products that act anticancer agents and others, [51–64] herein we adopted design and synthesis of new compounds containing thiazolidinone scaffold. Thiazolidinones **3a,b** were synthesized from the starting thiosemicarbazones **2a,b**, then **3a,b** undergoing Knövenagel condensation with different aryl and heteryl aldehydes by a two-step or multicomponent route to afford three series of thiazolidinones **5a-j**, **7a-h** and **9a-j** bearing substitution at position-5 (Fig. 3). Twelve of the newly synthesized products were examined for their cytotoxic activity towards MCF-7, HepG2 and

HeLa, besides the most potent compounds were evaluated against the normal WI-38 cell line detected their safety character toward normal human cells. Thiazolidinones **5c** and **5h**, the most potent anticancer candidates were evaluated as target protein kinase inhibitors against EGFR and their effects on the cell cycle and their ability to induce apoptosis in the HepG2 cell line were also investigated. A docking study was also operated to predict the binding modes of the compounds **5c** and **5h** within the binding site of EGFR using the PDB file (1M17 is the crystal structure of epidermal growth factor receptor with the co-crystallized ligand Erlotinib). Furthermore, *in silico* toxicity potential by Osiris methodology was performed on twelve synthesized compounds, all of which had zero toxicity risks and were predicted to have good physicochemical properties, thus compounds **5c** and **5h** were detected to be safe as drug candidates with favorable properties.

2. Experimental

2.1. Chemistry

General

The equipment used for detecting the spectral (IR, ^{1}H NMR, ^{13}C NMR and Mass) and physical analyses (melting points, and color) are provided in details in ESI. The elemental analyses and spectral analyses were carried out through the microanalytic center at Cairo University and microanalytic unit-FOPC-NMR Unit-Faculty of Pharmacy-Cairo University. The anticancer investigations were carried out at Faculty of Pharmacy-El Mansoura University. The aldehydes 4-formylphenyl benzoate **1a** and 4-formyl-2-methoxyphenyl benzoate **1b** were prepared according to the reported method. [65, 66]

Procedure for the synthesis of thiosemicarbazones 2a,b

An equimolar of the aldehydes **1a,b** (0.01 mol) and thiosemicarbazide (0.01 mol) was added to a solution of absolute ethanol (10 ml) and glacial acetic acid (3 drops), then the reaction mixture was refluxed for 4 hrs. The reaction mixture was cooled and filtered off then the product was recrystallized from ethanol-dioxane mixture.

Procedure for the synthesis of thiazolidinone derivatives 3a,b

Method A

Aldehydes **2a,b** (0.01 mol) was refluxed with choloroacetic acid (0.01 mol) and fused sodium acetate (0.01 mol) in glacial acetic acid (10 ml) for 4 hours. Thiazolidinones **3a,b** were collected through filtration, washed by ethanol and then recrystallized from glacial acetic acid.

Method B

Aldehydes **2a,b** (0.01 mol) refluxed with ethyl bromoacetate (0.01 mol) in pure ethanol (10 ml) containing fused sodium acetate (0.01 mol) for 4 hours. Thiazolidinone derivatives **3a,b** were collected through filtration and recrystallized from glacial acetic acid.

The detailed procedures and the spectral data together with the physical data for all the synthesized compounds were discussed in details in the ESI.

2.2. Biological activity

2.2.1. *In Vitro* Anticancer screening

MTT assay

It was operated in the Faculty of Pharmacy-El Mansoura University. The Cell lines used are HepG2, MCF-7, and HeLa and they are provided through VACSERA [Holding company for biological products and vaccines]. The MTT assay was conducted according to the literature. [67] The procedure is discussed in details in the ESI.

2.2.2 The inhibitory assay for EGFR kinase

Compounds **5c** and **5h**, were evaluated for their inhibitory activities against EGFR. The procedure is discussed in details in the ESI

2.2.3. Cell cycle by *In vitro* DNA-flow cytometric analysis

The first step in the technique is to prepare the HepG2 cells in 25 cm^2 cell culture flask. The compounds **5c** and **5h** were prepared at their IC_{50} that obtained from MTT assay then treated with RPMI-1640 medium separately. The procedure is discussed in details in the ESI.

2.2.4. The apoptosis assay by Annexin V-FITC analysis

HepG2 cells were harvested and incubated with compound **5c** and **5h** separately. The experiment was carried by the BioVision Annexin V-FITC Apoptosis Detection Kit. The procedure is discussed in details in the ESI.

2.3. Computational studies

2.3. 1. Molecular docking

The 2D structure of **5c** and **5h** was drawn through chemdraw program 2021 then each were saved as MDL Molfile (*.mol). The protonated 3D structure of **5c** and **5h** were applied to measure their bond lengths and angles in their binding pattern with the active site of the co-crystallized structure of EGFR protein kinase with its ligand erlotinib was downloaded (PDB code: 1M17) using MOE program version 2015[Molecular Operating Environment]. The co-crystallized structure of EGFR protein kinase with its ligand erlotinib was downloaded (PDB code: 1M17) from protein data bank ((www.rcsb.org/structure/1m17). The procedure is discussed in details in the ESI.

2.3.2. *In silico* toxicity potential.

Physicochemical characteristics and toxic hazards of **3-d, 5f, 5h**, **5i**, **7a**, **7e** and **9a** were detected through Osiris methodology [68] and the details were mentioned within the ESI.

3. Result And Discussion

3.1. Chemistry

Thiosemicarbazide reacted with each of 4-formylphenyl benzoate **1a** and 4-formyl-2-methoxyphenyl benzoate **1b** in ethanol containing a catalytic amount of glacial acetic acid afforded the corresponding thiosemicarbazones **2a,b**. In compound **2a**`s IR spectrum, there are bands at $\upsilon_{max}$ 3455 and 3285 $cm^{-1}$ for $NH_2$ and NH functions besides a band for carbonyl group at $\upsilon_{max}$ 1734 $cm^{-1}$. The $^1H$ NMR showed a *$D_2O$* broad signal at δ = 6.51 ppm for $NH_2$`s protons besides another singlet *D_2O* band at δ ~ 10.30 ppm for NH amide group`s proton. Additionally, there are three doublet bands at δ = 7.29, 7.80 and 8.12 ppm with *J* coupling; 8.7, 8.7 and 7.2 Hz, respectively, all together with another multiple signals at δ = 7.58–7.74 ppm for aromatic protons. Its ^{13}C NMR spectrum displayed significant signals at δ = 151.5, 157.2 and 165.0 ppm for CO, =CH and C = S respectively, with another expected signals at δ = 122.6, 128.2, 129.4, 129.5, 130.3, 133.2, 134.6 and 138.8. (See exp., Scheme 1).

Furthermore, the reaction of the thiosemicarbazones **2a,b** with chloroacetic acid in refluxing acetic acid containing equivalent amount of fused sodium acetate afforded the respective thiazolidinones **3a,b** (Scheme 2). In the IR spectrum of **3b**, presented a broad band at υ_{max} = 3421 cm^{-1} for imino group with other bands at υ_{max} = 1727 and 1633 cm^{-1} for carbonyl groups. The ^1H NMR spectrum of **3b** revealed singlet signals at δ = 3.81 and 3.88 ppm for $methoxy s \text{ and } methy \leq \neq$ s protons respectively, besides another three doublet signals at δ = 7.32, 7.61 and 8.11 ppm with *J* coupling; 8.1, 7.8 and 7.2 Hz, respectively. Also, the spectrum showed a *D_2O* singlet signal at δ ~ 12.01 ppm for NH`s proton, in addition to another expected signals for aromatic protons and a singlet signal at δ = 8.43 ppm for vinylic proton. Its $^{13}C$ NMR spectrum displayed significant signals at δ = 164.3, 155.8, 151.6, 56.3 and 33.5 ppm for two CO, C = N of the thiazolidinone ring, $OCH_3$`s and CH_2`s carbon respectively. The Mass spectrum of **3b** revealed a molecular ion peak at m/z = 369 (M^+, 4.55%) which was constituent with the molecular formula $C_{18}H_{15}N_3O_4S$ (See exp. Scheme 2). The thiazolidinones **3a,b** were prepared through another alternative method through the reaction of thiosemicarbazones **2a,b** with ethyl bromoacetate and equivalent amount of fused sodium acetate resulted in thiazolidinones **3a,b** after 4 hrs under reflux with better yield% [yield% of **3a**; 80 and yield% of **3b**; 78]. The physical aspects and spectral data for **3a,b** obtained by this method were similar as the method A.

Knövenagel condensation of thiazolidinones **3a,b** with different aryl or heteryl aldehydes **4a-e** in *N,N*-dimethylformamide concerning few drops of piperidine formed the corresponding arylidenes **5a-j** (Scheme 3). In the ^1H-NMR spectrum of **5d**, the CH_2`s protons at δ = 3.91 ppm were absent instead the two $OCH_3$`s protons appeared at δ = 3.80 and 3.85 ppm besides a *D_2O* exchangeable signal at δ = 12.65 ppm for imino proton, also another multiplet signals referred to aryl and vinylic signals at δ = 6.86–7.09 and 7.76–7.80 ppm, respectively, besides three doublet signals at δ = 7.44, 7.92 and 8.15 ppm with *J* coupling constants 8.0, 8.0 and 7.2 Hz, respectively. The IR spectrum for **5d** showed absorption bands at wavelengths 3433, 1738 and 1635 cm^{-1} for imino and carbonyl groups. There are significant signals in the ^{13}C NMR spectrum of **5d** at δ = 174.9, 164.8, 155.7, 153.4, 55.8 and 56.2 ppm for two CO, two C = N and two C-OCH_3 respectively, with another expected signals. The spectral data together with elemental data were in agreement with the suggested structures 5a-j (See exp. Scheme 3). The alternative pathway of the preparation of **5a-j** through multicomponent reaction (Method B). So an equimolar amounts of **2a,b**, chloroacetic acid and the aldehydes **4a-e** in refluxing glacial acetic acid containing fused sodium acetate afforded the same products of the above pathway (Method A) in all physical and spectral aspects (Scheme 3, See Table 1).

Furthermore, compounds **3a,b** were condensed with pyrazole-4-carbaldehyde derivatives **6a-d** delivering the respective arylidene derivatives **7a-h** according to method A (Scheme 4). The structures of **7a-h** were confirmed by spectral tools and elemental analyses, taken for example the spectral data for **7g**, its IR spectrum showed a broad band at v_{max} = 3422 cm^{-1} for NH group and bands at v_{max} 1728 and 1648 cm^{-1} for carbonyl groups. In its ^{1}H-NMR spectrum there are two singlet signals at δ = 3.85 and 3.91 ppm for two methoxy protons and a *D_2O* exchangeable singlet signal at δ = 12.55 ppm due to NH proton, with another expected multiplet signals at δ = 7.34-7.54 and 7.69-7.80 ppm for aryl protons besides doublet signals were found at d = 7.56, 7.60, 7.66, 8.03 and 8.14 ppm with *J* coupling constants 7.6, 7.6, 7.2, 7.6 and 7.2 Hz, repetitively besides two singlet signals at d = 8.44 and 8.84 ppm for vinylic protons and one singlet signal at d = 8.56 ppm for pyrazole`s proton. Alternatively, the arylidene derivatives **7a-h** were obtained through the multicomponent reaction through three components: **2a,b**, chloroacetic acid and the pyrazole-4-carbaldehydes **6a-d** in refluxing glacial acetic acid and fused sodium acetate (Method B) affording the same products of the above two step pathway similar in the physical and spectral aspects in different yield% (See Table 1, See Exp. Scheme 4).

Furthermore, compounds **3a,b** were condensed with pyrazole-4-carbaldehyde derivatives **6a-d** delivering the respective arylidene derivatives **7a-h** according to method A (Scheme 4). The structures of **7a-h** were confirmed by spectral tools and elemental analyses, taken for example the spectral data for **7g**, its IR spectrum showed a broad band at v_{max} = 3422 cm^{-1} for NH group and bands at v_{max} 1728 and 1648 cm^{-1} for carbonyl groups. In its ^{1}H-NMR spectrum there are two singlet signals at δ = 3.85 and 3.91 ppm for two methoxy protons and a *D_2O* exchangeable singlet signal at δ = 12.55 ppm due to NH proton, with another expected multiplet signals at δ = 7.34–7.54 and 7.69–7.80 ppm for aryl protons besides doublet signals were found at δ = 7.56, 7.60, 7.66, 8.03 and 8.14 ppm with *J* coupling constants 7.6, 7.6, 7.2, 7.6 and 7.2 Hz, repetitively besides two singlet signals at δ = 8.44 and 8.84 ppm for vinylic protons and one singlet signal at δ = 8.56 ppm for pyrazole`s proton. Alternatively, the arylidene derivatives **7a-h** were obtained through the multicomponent reaction through three components: **2a,b**, chloroacetic acid and the pyrazole-4-carbaldehydes **6a-d** in refluxing glacial acetic acid and fused sodium acetate (Method B) affording the same products of the above two step pathway similar in the physical and spectral aspects in different yield% (See Table 1, See Exp. Scheme 4).

Finally, under the same reaction conditions of method A, the condensation of compounds **3a,b** with 5-arylazo-2-hydroxybenzaldehydes **8a-e** afforded the respective arylidenes **9a-j** (Scheme 5). The IR spectrum of **9c** exposed absorption bands appeared at υ_{max} 3412 and 3242 cm^{-1} attributed to imino and hydroxyl functions, also absorption bands at υ_{max} 1736 and 1637 cm^{-1} attributed to CO functions, respectively. In the ^{1}H NMR spectrum of **9c** there are five doublet signals at δ 6.81, 7.13, 7.47, 7.92 and 8.13 ppm for aryl protons with *J* coupling constants = 8.1, 8.4, 8.1, 8.1 and 8.4 Hz and a multiplet signal at 7.30–7.44 ppm and 7.52–7.88 ppm for phenyl protons, and two exchangeable *D_2O* signals at = 9.97 and 11.91 ppm due to imino and hydroxyl protons. Additionally, there were two singlet signals at δ 8.26 and 8.56 ppm due to vinylic protons. The products **9a-j** were obtained also alternatively through one-pot reaction of **2a,b**, chloroacetic acid and arylazo salicyladehydes **8a-e** (Method B) (See Table 1, Scheme 5).

Table 1 Yield% of **5a-j, 7a-h** and **9a-j** obtained by Method **A** and Method **B** revealing the reaction time in each method

Compound No.	Method A		Method B	
	Yield%	Time (hrs)	Yield%	Time (hrs)
5a	70	4	90	9
5b	78	4	70	9
5c	78	4	78	10
5d	78	5	76	12
5e	55	6	52	14
5f	86	4	80	14
5g	74	5	72	12
5h	55	5	58	12
5i	64	6	60	12
5j	78	6	72	14
7a	75	6	78	12
7b	78	6	75	12
7c	78	6	76	15
7d	78	6	70	14
7e	52	6	60	14
7f	78	6	68	14
7g	68	6	68	13
7h	80	6	76	18
9a	78	4	80	12
9b	73	4	78	12
9c	80	5	78	12
9d	52	6	68	16
9e	78	6	88	16
9f	64	6	70	14
9g	56	6	68	14
9h	54	6	70	18
9i	88	6	82	18
9j	58	6	74	18

3.2. Biological activities

3.2.1. Cytotoxic activity assessment by *in vitro* MTT assay

The tested compounds` cytotoxicity and anticancer activity against MCF-7, HepG2 and HeLa was detailed in Table 2. The MTT assay was used for screening the anticancer activity of the tested compounds. [67] Furthermore, these compounds were examined against normal lung fibroblast (WI38) to find if they are safe towards the normal cells. Sorafenib was used as a reference drug and the obtained data for the cytotoxicity of the compounds in the three cell lines (IC_{50}, μM) was detailed in Table 2. According to the revealed data the compounds under test displayed versatile anticancer activity toward the three cell lines showing moderate to very strong activity. The starting thiazolidinones **3a** and **3b** showed strong activity in MCF-7, HepG2 and HeLa with IC_{50} values for **3a**; 17.26 ± 1.5, 14.50 ± 1.1 and 11.66 ± 0.9 μM, respectively, while IC_{50} for **3b**; 17.71 ± 1.4 and 21.26 ± 1.5 μM in MCF-7 and HepG2, respectively. Compound **3b** exhibited weak anticancer activity in HeLa with IC_{50} = 50.67 ± 2.8 μM. The compound **5c** showed high potency in HepG2 and HeLa with IC_{50}; 9.15 ± 0.6 and 9.18 ± 0.7 μM, respectively. Compared with sorafenib, **5c** was

more potent in HepG2 with IC_{50} which was in an equipotent manner to sorafenib (IC_{50}; 9.18 ± 0.6 µM). The compound **5h** produced the most significant cytotoxic activity towards the cell lines under study among all the tested compounds. It showed more potency than the standard in HepG2 and HeLa with IC_{50} values; 6.22 ± 0.4 and 9.18 ± 0.7 µM, respectively, comparing with sorafenib with IC_{50} values; 9.18 ± 0.6 and 8.04 ± 0.5 µM, respectively. The presence of 4-methoxyphenyl moiety in the thiazolidinone ring of **5c** and **5h** produced enhancement in the anticancer activity.

The most active compounds **3a**, **3b**, **5a**, **5c** and **5h** were examined for their cytotoxicity against the normal fibroblasts (WI38) cell line. The tested compounds showed higher IC_{50} towards WI38 cell lines as they had cytotoxicity with IC_{50}; 80.07 ± 3.9, 83.87 ± 4.1, 38.20 ± 2.4, 79.30 ± 3.7 and 57.54 ± 3.2 µM for **3a**, **3b**, **5a**, **5c** and **5h**, respectively. From these results, it was concluded that **3a**, **3b**, **5a**, **5c** and **5h** can be used as anticipated anticancer agents targeting only the cancerous cells (Table 2, Fig. 4).

Table 2
Showed MTT anticancer assessment of some products against HepG2, MCF-7, HeLa and WI38 using sorafenib as a standard drug

3a	**14.50 ± 1.1**	**17.26 ± 1.5**	**11.66 ± 0.9**	**80.07 ± 3.9**
Sorafenib	**9.18 ± 0.6**	**7.26 ± 0.3**	**8.04 ± 0.5**	**10.65 ± 0.8**
Compound NO.	**Cell line (HepG2) IC_{50} (µM)**	**Cell line (MCF-7) IC_{50} (µM)**	**Cell line (HeLa) IC_{50} (µM)**	**Cell line (WI38) IC_{50} (µM)**
3b	**21.26 ± 1.5**	**17.71 ± 1.4**	**50.67 ± 2.8**	**83.87 ± 4.1**
5a	**26.98 ± 1.9**	**20.73 ± 1.8**	**19.07 ± 1.4**	**38.20 ± 2.4**
5b	**31.47 ± 2.1**	**25.50 ± 2.0**	**86.01 ± 4.0**	
5c	**9.15 ± 0.6**	**13.55 ± 1.1**	**9.18 ± 0.7**	**79.30 ± 3.7**
5d	**43.18 ± 2.6**	**35.08 ± 2.3**	**36.59 ± 2.2**	
5f	**98.90 ± 4.4**	**51.98 ± 2.9**	**74.30 ± 3.6**	
5h	**6.22 ± 0.4**	**9.39 ± 0.7**	**7.78 ± 0.5**	**57.54 ± 3.2**
5i	**52.27 ± 2.9**	**36.24 ± 2.4**	**30.89 ± 2.1**	
7a	**78.65 ± 3.6**	**45.15 ± 2.7**	**59.98 ± 3.3**	
7e	**108.60 ± 4.8**	**63.96 ± 3.3**	**64.05 ± 3.4**	
9a	**63.86 ± 3.2**	**41.38 ± 2.5**	**23.79 ± 1.9**	

IC_{50}: Compound concentration required to cause cell death by 50%, IC_{50} values = mean ± SD

3.2.2. The Inhibitory activity of compounds 5c and 5h towards EGFR tyrosine kinase.

The most cytotoxic products **5c** and **5h** were examined as target protein kinase inhibitors for EGFR tyrosine kinase and erlotinib was used as standard drug. [69, 70] The obtained data was summarized in Table 3. Compound **5c** showed decrease in the inhibitory activity against EGFR kinase protein with IC_{50} value; 0.2 µM compared to the reference drug erlotinib which had IC_{50} value; 0.037 µM. While, the thiazolidinone derivative **5h** appeared to be more potent inhibitor against EGFR kinase activity giving IC_{50} value; 0.098 µM. It could be noticed that the presence of donating substitution in the pharmacophore of **5c** and **5h** caused a positive effect in the inhibition against EGFR kinase and the increase in the number of that kind of substitution in turn increased the inhibitory effect as seen in **5h**. [71]

Table 3 Revealed data of inhibitory investigation of compounds 5c and 5h for EGFR tyrosine kinase using erlotinib as a standard drug	
Cpd. No.	**EGFR IC_{50} (mean ± SD) µM**
Erlotinib	**0.037 ± 0.002**
5c	**0.2 ± 0.009**
5h	**0.098 ± 0.004**
IC_{50}: Compound concentration required to cause enzyme inhibition by 50%, IC_{50} values = mean ± SD (standard deviation)	

3.2.3. Cell cycle analysis for 5c and 5h by DNA-flow cytometric assay

Moreover, the compounds **5c** and **5h** were evaluated for their effect on the cell cycle in HepG2 cell lines. The stages of cell cycle were detected through flow cytometry after propidium iodide (PI) staining [69]. From the obtained results, it was concluded that **5c** and **5h** caused interruption in the cell cycle progression in the treated HepG2 cells. The change in the cell content % was detected in the treated cells with **5c** and **5h** compared to the control cells. It was observed that the content of the cells at pre-G1 stage increased in the treated HepG2 cells from 44.41–52.48% a decrease in the quantity of cells at S phase and G2/M phase from in 35.49% and 19.7% (Fig. 5, B) so that it was clearly detected that **5c** arrested the cell cycle in G1 phase. While treatment of HepG2 cells with **5h**, there was an increase in the quantity of cells was observed at pre-G1 and S phases to reach 47.22% and 42.04%, respectively causing a remarkable decrease in the cell content in the G2/M phase to reach 10.74% in treated cells, for that observation, it was clear that **5h**arrested the cell cycle at the late G1 phase and the beginning of S phase (Fig. 5, C).

3.2.4. Determination of apoptosis induction for 5c and 5h by annexin V-FTTC method

The cell death of HepG2 cell line by apoptotic pathway induced by compound **5c** and **5h** was determined by annexin V/PI assay [69]. Annexin V-FITC stain was used to stain cells with PI dye. The principle of this method is the cells that are in the late apoptosis stage are stained positive with V/PI. The HepG2 cells were treated with compounds **5c** and **5h** at their IC_{50} concentrations 9.15 ± 0.6 and 6.22 ± 0.4 µM, respectively for 24 hr after that the cells were stained by annexin V / PI and then the corresponding red PI and green FITC fluorescence was detected by flow cytometry technique. The representative dot plots for compounds **5c** and **5h** of flow cytometric analyses showing four various distributions (Fig. 6). After treatment with **5c**, 11.93% of the cells were in early apoptosis and 21.95% were in a late apoptosis phase, respectively (Table 5, Fig. 6, B). While cells treated with **5h** revealed that 28.51% of the cells were in early apoptosis and 16.36% were in a late apoptosis phase, respectively (Fig. 6, C). As concluded, the cell death of the treated HepG2 cells was caused mainly by apoptosis after treatment with compounds **5c** and **5h**as low content of these cells was in necrosis stage.

Table 4 Revealed cell content% of HepG2 treated cells by 5c and 5h obtained from cell cycle analysis			
Compound No.	**DNA Content**		
	%G0-G1	**%S**	**%G2/M**
5c / HepG2	**52.48**	**31.66**	**15.86**
5h / HepG2	**47.22**	**42.04**	**10.74**
Cont. HepG2	**44.81**	**35.49**	**19.7**

Table 5 Displayed the cell percentage of apoptosis and necrosis induction of HepG2 treated by 5c and 5h obtained by annexin V-FTTC/ PI assay				
Cpd. No.	**Apoptosis**			**Necrosis**
	Total	**Early**	**Late**	
5c /HepG2	**42.16**	**11.93**	**21.95**	**8.28**
5h /HepG2	**51.39**	**28.51**	**16.36**	**6.52**
cont. HepG2	**2.33**	**0.61**	**0.19**	**1.53**

3.3. Computational studies

3.3.1. Molecular modeling and Docking Study on EGFR

The anticancer investigated compounds **5c** and **5h** were subjected for Molecular docking using Molecular operating environment [MOE dock 2015] software. The docking studies were subjected to determine the possible binding pattern between the 3D structure of **5c** and **5h** with the active site pocket of EGFR kinase. The self-docking of the active site of EGFR with the co-crystallized ligand erlotinib (PDB code: 1M17) has an energy score of -7.8094 Kcal mol^{-1} and RMSD value of 0.9361Å between erlotinib and its docked pose. As depicted in Fig. 7, the compound **5c** was bonded to the active site of EGFR with energy score − 11.9196 Kcal mol^{-1} and RMDS value 1.3455 Å with the formation of hydrogen-arene interaction through the thiazolidinone centroid and the amino acid Gly 772 with bond length equal 3.67 Å.

By inspection of Fig. 8, the derivative **5h** was bonded to the vicinity of EGFR $activesitewiththef \text{ or } mationofo \neq hydro \geq nbondaep \rightarrow rbetweenthe \otimes y \geq na \rightarrow mofcarbonylgroup \text{ and } thebackbo \neq$ s amino acid Thr 830 with bond length value 2.59 Å. The energy score of the interaction was − 12.1942 Kcal mol^{-1} and the RMDS value 1.7160 Å.

Finally, regarding to the superimposition Fig. 7A and 8A, it was noted that the presence of thiazolidinone ring in compound **5c** and the presence of carbonyl group in **5h** gave a chance for better insertion of these compounds into the active site of EGFR with similar bonding pattern as the co-crystallized ligand erlotinib through hydrogen-arene and hydrogen bond formations.

3.3.1. *In silico* toxicity potential by Osiris property explorer

The newly synthesized compounds **3a**, **3b**, **5a**, **5b**, **5c**, **5d**, **5f**, **5h**, **5i**, **7a**, **7e** and **9a** were examined for detecting their toxic effects such as mutagenic, tumorigenic properties and skin irritants besides predicting their physicochemical properties via Osiris methodology, [68] and the obtained results were detailed in Table 6. From the obtained results, it was concluded that all the compounds under study have no tendency to be mutagenic, tumorigenic or even cause skin irritation and have no reproductive effect except compound **9a** which showed to have toxicity risks. The compounds **3a** and **3b** showed to have a better drug score of values; 0.61 and 0.6 respectively with better TPSA values that are $\leq$140 Å (**3a** has TPSA = 105.4 Å, **3b** has TPSA = 114.6 Å). Compound **5a** has drug score = 0.3 and TPSA value; 105.4 Å. The most cytotoxic compounds **5c** and **5h** showed to have almost the same drug score of values; 0.29 and 0.28 respectively with TPSA values; 114.6 Å and 123.8 Å, respectively. The compounds **5c** and **5h**showed their effectiveness and potentiality as new drugs.

Table 6
Predicted toxicity risks and physicochemical properties obtained according to Osiris property explorer software

Comp. no.	*Mutagenicity*	*Tumorgenicity*	*Irritancy*	*Reproductive effect*	*Solubility*	*Drug-likeness*	*Drug score*	*TPSA*
	Toxicity risks							
3a	Green	Green	Green	Green	-4.98	4.35	0.61	105.4
3b	Green	Green	Green	Green	-5.0	5.59	0.6	114.6
5a	Green	Green	Green	Green	-6.81	4.35	0.3	105.4
5b	Green	Green	Green	Green	-7.55	6.04	0.25	105.4
5c	Green	Green	Green	Green	-6.83	5.43	0.29	114.6
5d	Green	Green	Green	Green	-6.85	6.05	0.28	123.8
5f	Green	Green	Green	Green	-6.83	5.53	0.29	114.6
5h	Green	Green	Green	Green	-6.85	6.82	0.28	123.8
5i	Green	Green	Green	Green	-6.86	6.85	0.26	133.1
7a	Green	Green	Green	Green	-8.32	7.52	0.19	123.2
7e	Green	Green	Green	Green	-8.34	8.59	0.18	132.4
9a	Red	Red	Orange	Red	-9.01	-2.94	0.02	150.3
Green color: shows less toxic, Orange color: shows mid toxic, Red color: shows high tendency of toxicity								

Conclusion

This research detailed synthesis of three series of thiazolidinone derivatives based on 4-formylphenyl benzoate **1a** and 4-formyl-2-methoxyphenyl benzoate **1b** as key precursors and most of these compounds were subjected for MTT assay for investigating their cytotoxicity towards three human cancer cell lines; hepatocellular HepG2, breast MCF-7 and cervical HeLa, using sorafenib as a reference standard. The compounds **5c** and **5h** revealed better inhibitory activities towards the three cancer cell lines with IC_{50} values for **5c**; 9.15, 13.55 and 9.18 µM in HepG2, MCF-7 and HeLa, respectively and IC_{50} values for **5h**; 6.22, 9.39 and 7.78 µM in HepG2, MCF-7 and HeLa, respectively, comparing to sorafenib of IC_{50}; 9.18, 7.26 and 8.04 µM in HepG2, MCF-7 and HeLa, respectively. Moreover, compounds **5c** and **5h** revealed an excellent safety pattern against the normal WI38 cell line. Additionally, compounds **5c** and **5h** were examined as targeting protein kinase inhibitors against EGFR, the compound **5c** showed inhibitory suppression effect of IC_{50}; 0.2 µM while **5h** showed potent inhibition impact of IC_{50}; 0.098 µM, comparing to the standard erlotinib of IC_{50}; 0.037 µM. Additionally, both **5c** and **5h** were investigated for their effect on cell cycle progression and induction of cell death by apoptosis in treated HepG2 cells and it was observed their ability in interrupting the cell cycle progression as **5c** arrested it in G1 phase and **5h** arrested it in the end of G1 phase and the start of S phase and all together caused cell death by apoptosis mechanism. Molecular docking study declared good fitting patterns with good binding energy in the active site of EGFR kinase protein [PDB file: 1M17], in addition toxicity study using Osiris property explorer revealed excellent drug like properties and no toxicity or hazards in humans.

Declarations

Competing interests

The authors declare no conflict of interest.

Authors' contributions

Nadia Hanafy Metally has generally supervised the work and has provides the conceptions, follow the data interpretations, original manuscript writing and reviewing process handling.

Salwa Magdy Eldaly has provides the conceptions, follow the analyses, data interpretations, original manuscript writing

Dalia salama has performed the experimental work, carried out the needed analysis and data presentation.

Availability of data and materials

The supporting information contains detailed experimental procedures, physical properties [Color, Yield%, m.p], spectroscopic data [IR, ^{1}H NMR, ^{13}C NMR and MS], elemental analyses of the compounds are found in the Supporting Information together with ^{1}H NMR spectra, ^{13}C NMR spectra, IR and MS spectra of some compounds are found.

References

1. A. M. Soliman, A. S. Alqahtani, M. M. Ghorab, Journal of Enzyme Inhibition and Medicinal Chemistry. **34**, 1030 (2019).
2. J. Ferlay, M. Laversanne, M. Ervik, F. Lam, M. Colombet, L. Mery, M. Pineros, A. Znaor, I. Soerjomataram, F. Bray, Global Cancer Observatory: Cancer Tomorrow, Lyon, France. (International Agency for Research on Cancer, 2020), https://gco.iarc.fr/tomorrow.
3. S. O. Zaraei, R. M. Sbenati, N. N. Alach, H. S. Anbar, R. ElGamal, H. Tarazi, M. K. Shehata, M. S. Abdel-Maksoud, C.-H. Oh, M. I. El-Gamal, Eur. J. Med. Chem. **224**, 113674 (2021).
4. H. Sung, J. Ferlay, R. L. Siegel, M. Laversanne, I. Soerjomataram, A. Jemal, F. Bray. CA Cancer J Clin.**71**, 209 (2021).
5. International Agency for Research on Cancer. (GLOBOCAN IARC 12 sept 2018), https://www.uicc.org/news/global-cancer-data-globocan-2018.
6. R. Awasthi, A. Roseblade, P. M. Hansbro, M. J. Rathbone, K. Dua, M. Bebawy, Curr. Drug Targets. **19**, 1696 (2018).
7. V.V. Padma, Biomedicines. **5**, 1 (2015).
8. Z. Du, C. M. Lovly, Mol. Cancer. **17**, 58 (2018).
9. N. Iqbal, N. Iqbal, Chemother. Res. Pract. **2014**, 357027 (2014).
10. B. J. Druker, Trends Mol. Med. **8**, S14 (2002).
11. K. S. Bhullar, N. O. Lagar´on, E. M. McGowan, I. Parmar, A. Jha, B. P. Hubbard, H. V. Rupasinghe, Mol. Cancer. **17**, 1 (2018).
12. H. Kittler, P. Tschandl, Br. J. Dermatol. **178**, 26 (2018).
13. A. Ayati, S. Moghimi, S. Salarinejad, M.Safavi, B. Pouramiri, A.Foroumadi, Bioorg. Chem. **99**, 103811 (2020).
14. E.-M. Birkman, A.Ålgars, M. Lintunen, R. Ristamaki, J. Sundstrom, O.Carpén, BMC Cancer. **16**, 406 (2016).

15. M. D. Siegelin, A. C. Borczuk, Laboratory Investigation. **94**, 129 (2014).
16. C. B. Williams, K. Phelps-Polirer, I. P. Dingle, C. J. Williams, M. J. Rhett, S. T. Eblen, K. Armeson, E. G. Hill, E. S. Yeh, Oncogene. **39**, 1112 (2020).
17. X. Yang, W. Wang, C. Wang, L. Wang, M. Yang, M. Qi, H. Su, X. Sun, Z. Liu, J. Zhang, X. Qin, B. Han, Oncology Reports. **32**, 700 (2014).
18. N. Normanno, M. R. Maiello, A. De Luca, J. Cell Physiol. **194**, 13 (2003).
19. Y. Ito, T. Takeda, M. Sakon, M. Tsujimoto, S. Higashiyama, K. Noda, E. Miyoshi, M. Monden, N. Matsuura, Br J Cancer. **84**, 1377 (2001).
20. S. Kira, T. Nakanishi, S. Suemori, M. Kitamoto, Y. Watanabe, G. Kajiyama, Liver. **17**, 177 (1997).
21. G. Giannelli, A. Azzariti, C. Sgarra, L. Porcelli, S. Antonaci, A. Paradiso, Biochem Pharmacol. **71** (4), 479 (2006).
22. M. Hopfner, A. P. Sutter, A. Huether, D. Schuppan, M. Zeitz, H. Scherubl, J Hepatol. **41**, 1008 (2004).
23. A. Huether, M. Höpfner, V. Baradari, D. Schuppan, H. Scherübl, Biochem Pharmacol. **70**, 1568 (2005).
24. P. A. Philip, M. R. Mahoney, C. Allmer, J. Thomas, H. C. Pitot, G. Kim, R. C. Donehower, T. Fitch, J. Picus, C. Erlichman, J Clin Oncol. **23**, 6657 (2005).
25. R. Kannangai, F. Sahin, M. S. Torbenson, Modern Pathology. **19**, 1456 (2006).
26. M. R. V. Finlay, R. A. Ward, the Topics in Medicinal Chemistry, (Springer, 28, 2017), pp. 39.
27. S. O. Lim, C. W. Li, W. Xia, H. H. Lee, S. S. Chang, J. Shen, J. L. Hsu, D. Raftery, D. Djukovic, H. Gu, W. C. Chang, H. L. Wang, M. L. Chen, L. Huo, C. H. Chen, Y. Wu, A. Sahin, S. M. Hanash, G. N. Hortobagyi, M. C. Hung, Cancer Res. **76**, 1284 (2016).
28. H.-Y. Lin, W.-X. Sun, C.-S. Zheng, H.-W. Han, X. Wang, Y.-H. Zhang, H.-Y. Qiu, C.-Y. Tang, J.-L. Qi, G.-H. Lu, R.-W.Yang, X.-M. Wang, Y.-H. Yang, RSC Adv. **7**, 48404 (2017).
29. Y. Yarden, G. Pines, Nat Rev Cancer. **12**, 553 (2012).
30. R. R. Khattab, A. A. Hassan, D. A. A. Osman, F. M. AbdelMegeid, H. M. Awad, E. S. Nossier, W. A. El-Sayed, Nucleosides, Nucleotides Nucleic acids. **40**, 1090 (2021).
31. F. Ciardiello, G. Tortora, Clin. Cancer Res. **7**, 2958 (2001).
32. A. Ayati, S. Moghimi, S. Salarinejad, M. Safavi, B. Pouramiri, A. Foroumadi, Bioorg. Chem. **99**, 103811 (2020).
33. R. R. Khattab, A. K. Alshamari, A. A. Hassan, H. H. Elganzory, W. A. El-Sayed, H. M. Awad, E. S. Nossier, N. A. Hassan, J. Enzyme Inhib. Med. Chem. **36**, 504 (2021).
34. I. M. Othman, Z. M. Alamshany, N. Y. Tashkandi, M. A. Gad-Elkareem, M. M. Anwar, E. S. Nossier, Bioorg. Chem. **114**, 105078 (2021).
35. N. Ahangar, A. Ayati, E. Alipour, A. Pashapour, A. Foroumadi, S. Emami, Chemical Biology & Drug Design. **78**, 844 (2011).
36. A. Ayati, S. Emami, A. Asadipour, A. Shafiee, A. Foroumadi, European Journal of Medicinal Chemistry. **97**, 699 (2015).
37. M. Djukic, M. Fesatidou, I. Xenikakis, A. Geronikaki, V. T. Angelova, V. Savic, M. Pasic, B. Krilovic, D. Djukic, B. Gobeljic, M. Pavlica, A. Djuric, I. Stanojevic, D. Vojvodic, L. Saso, Chemico-Biological Interactions. **286**, 119 (2018).
38. N. B. Patel, H. R. Patel, F. M. Shaikh, D. Rajani, Medicinal Chemistry Research. **23**, 1360 (2014).
39. K. A. Szychowski, M. L. Leja, D. V. Kaminskyy, U. E. Binduga, O. R. Pinyazhko, R. B. Lesyk, J. Gminski, Chemico-Biological Interactions. **262**, 46 (2017).
40. A. Leoni, A. Locatelli, R. Morigi, M. Rambaldi, Expert Opinion on Therapeutic Patents. **24**, 759 (2014).
41. G. M. Keating, Drugs. **77**, 85 (2017).
42. A. Puszkiel, G. Noé, A. Bellesoeur, N. Kramkimel, M.-N. Paludetto, A. Thomas-Schoemann, M. Vidal, F. Goldwasser, E. Chatelut, B. Blanchet, Clinical Pharmacokinetics. **58**, 451 (2019).
43. P. C. Lv, H. Q. Li, J. Sun, Y. Zhou, H. L. Zhu, Bioorg. Med. Chem. **18**, 4606 (2010).
44. P. C. Lv, D. D. Li, Q. S. Li, X. Lu, Z. P. Xiao, H. L. Zhu, Bioorg. Med. Chem. Lett. **21**, 5374 (2011).
45. K. Vaarla, R. K. Kesharwani, K. Santosh, R. R. Vedula, S. Kotamraju, M. K. Toopurani, Bioorg. Med. Chem. Lett. **25**, 5797 (2015).
46. P. A. Channara, M. Azizb, S. A. Ejazb, G.-e-S. Chaudhryc, A. Saeedb, R. Ujand, A. Hasana, S. R. Ejaze, A. Saeed, JOURNAL OF BIOMOLECULAR STRUCTURE AND DYNAMICS. (2021) https://doi.org/10.1080/07391102.2021.2018045
47. A. Kryshchyshyn-Dylevych, L. Radko, N. Finiuk, M. Garazd, N. Kashchak, A. Posyniak, K. Niemczuk, R. Stoika, R. Lesyk, Bioorganic & Medicinal Chemistry. **50**, 116453 (2021).
48. I. M. M. Othman, Z. M. Alamshany, N. Y. Tashkandi, M. A. M. Gad-Elkareem, S. S. Abd El-Karim, E. S. Nossier, RSC Adv. **12**, 561 (2022).
49. N. A. Khalil , E. M. Ahmed , H. B. El-Nassan, Med Chem Res. **22**, 1021 (2013).
50. K. El-Adl, H. Sakr, M. Nasser, M. Alswah, F. M.A. Shoman, Arch. Pharm. **353**, e2000079 (2020).
51. N. H. Metwally, M. A. Abdallah, M. A. Mosselhi, E. A. El-Desoky, Carbohydrate Research. 345, 1135 (2010).
52. N. H. Metwally, M. A. Badway, D. S. Okpy, Chem Pharm Bull. **63**, 495 (2015).
53. N. H. Metwally, F. M. Abdelrazek, S. M. Eldaly, Res Chem Intemed. **42**, 1071 (2016).

54. N. H. Metwally, E. A. Deeb, Bioorg. Chem. 77, 203 (2018).
55. N. H. Metwally, F. M. Abdelrazek, S. M. Eldaly, J. Heter. Chem. **45**, 2668 (2018).
56. N. H. Metwally, I. T. Radwan, W. S. El-Serwy, M. A. Mohamed, Bioorg. Chem. **84**, 456 (2019).
57. N. H. Metwally, M. S. Mohamed, E. A. Ragab, Bioorg. Chem. **88**, 102929 (2019).
58. N. H. Metwally, G. R. Saad, E. A. Abdwahab Int. J. Nanomed. **20**, 6645 (2019).
59. N. H. Metwally, F. M. Abdelrazek, S. M. Eldaly, J. Heter. Chem. **57**, 3653 (2020).
60. N. H. Metwally, S. O. Abdallah, M. M. Mohsen, Biorg. Chem. **97**, 103672 (2020).
61. N. H. Metwally, M. S. Mohamed,E. A. Deeb, Res. on Chem. Intermed. **47**, 5027 (2021).
62. N. H. Metwally, A. S. Abd-Elmoety, J. Molecular Str. **1257**, 132590 (2022).
63. N. H. Metwally, M. A. Badawy, D. S. Okpy, J. Mol. Str. **1258**, 132848 (2022).
64. N. H. Metwally, S. M. Eldaly, Chemistry Select (2022) https: //doi.org/ 10.1002/ slct.202202257.
65. Current Patent Assignee: ROKA FURADADA - WO2011/45389, 2011, A1.
66. N. H. Metwally, M. A. Badway, D. S. Okpy, Synth. Commun. **48**, 2496 (2018).
67. T. Mosmann. J. Immunol. Methods. **65**, 55 (1983).
68. The OSIRIS property explorer software. Available from: http://www.organic-chem istry.org/prog/peo/.
69. M. S. Nafie, S. M. Kishk, S. Mahgoub, A. M. Amer, Chem. Biol. Drug Des. **99**, 547 (2022).
70. M. W. Aziz, A. M. Kamal, K. O. Mohamed, A. A. Elgendy, Bioorg. Med. Chem. Lett. **41**, 127987 (2021).
71. O. M. Soltan, M. E. Shoman, S. A. Abdel-Aziz, K. Nagaoka, A. Narumi, M. Abdel-Aziz, J. Adv. Biomed. & Pharm. Sci. **4**, 152 (2021).

Schemes

Schemes are available in the Supplementary Files section.

Figures

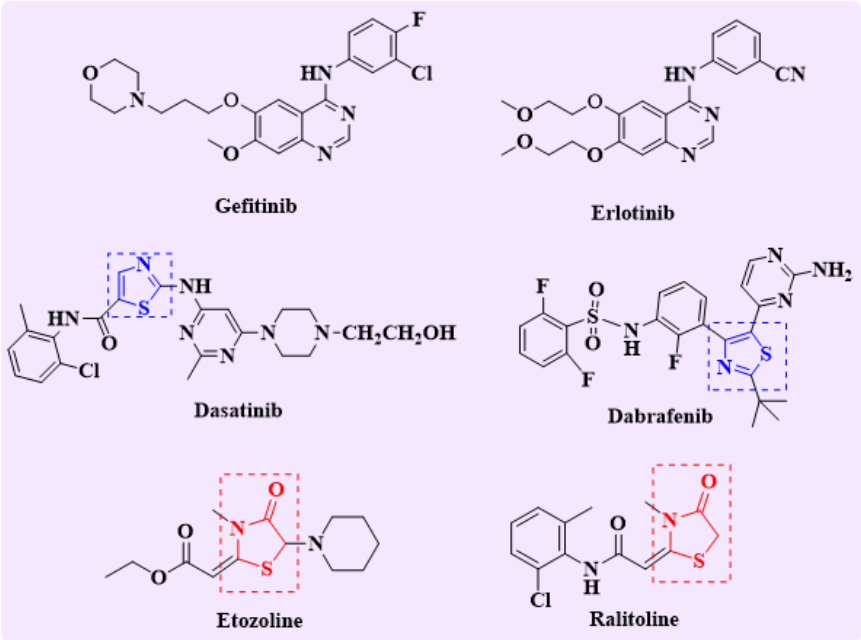

Figure 1

Reported EGFR inhibitors (Gefitinib and Erlotinib), antitumor agents and approved drugs containing thiazole and thiazolidinone core

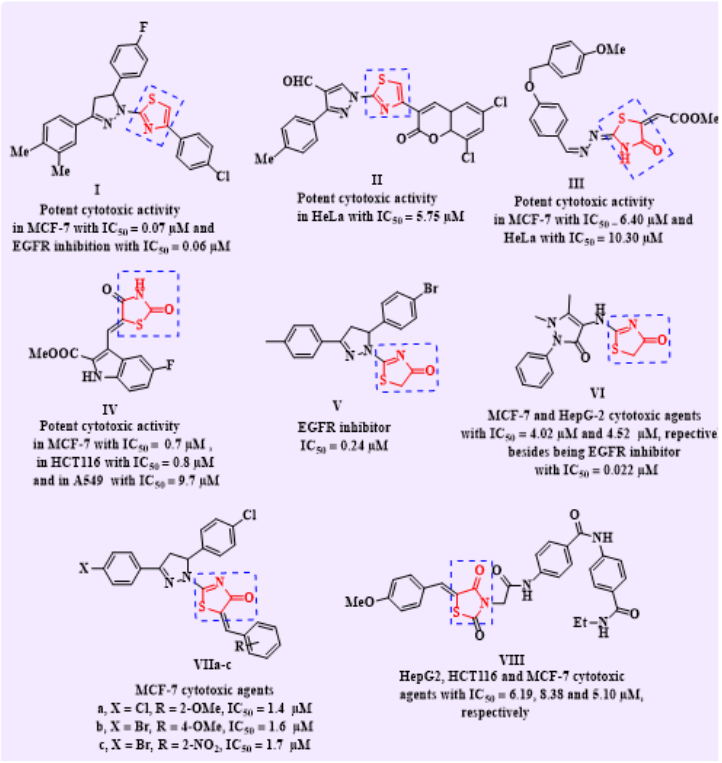

Figure 2

Examples of various EGFR inhibitors and antitumor agents containing thiazole ring

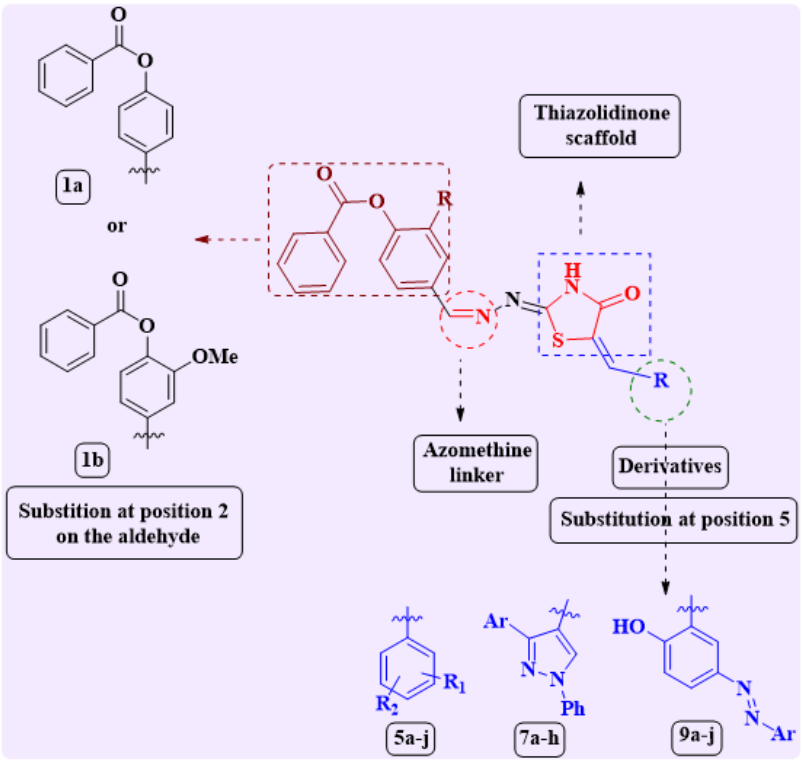

Figure 3

Molecular design of compounds depending on the thiazolidinones **3a,b**

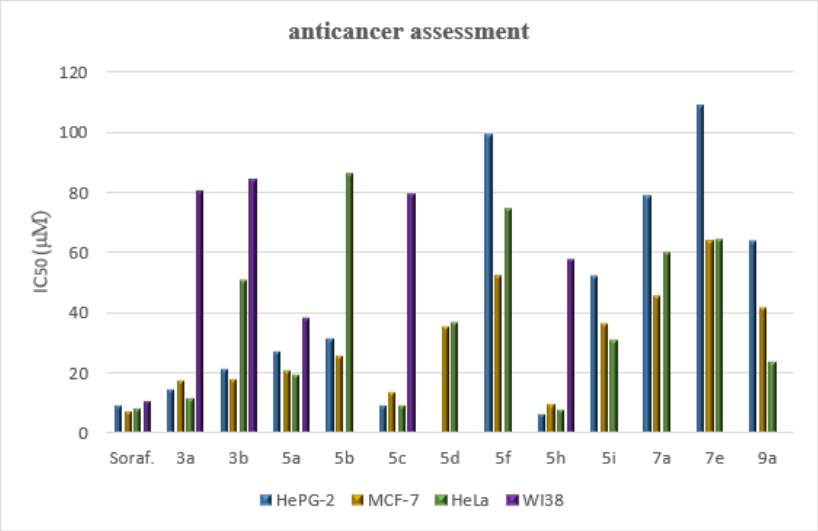

Figure 4

Cytotoxic activity assessment for target compounds

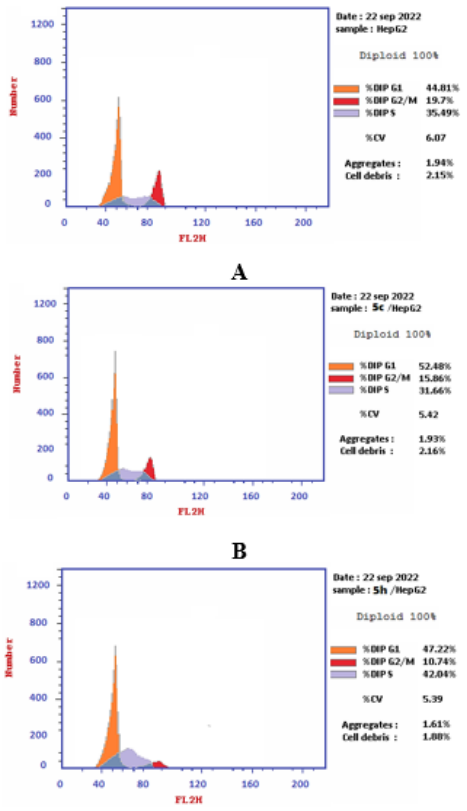

Figure 5

Cell cycle analysis of HepG2 treated by **5c (B)** and **5h (C)** by flow cytometry assay together with the untreated HepG2**(A)**

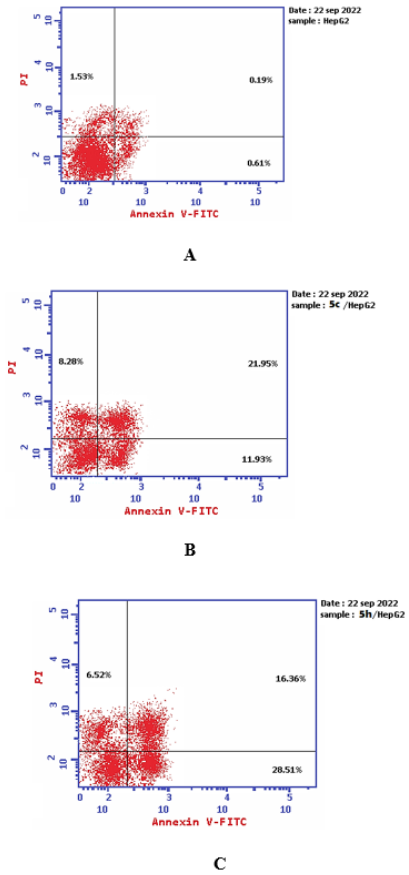

Figure 6

A representative plot of apoptosis induction of HepG2 treated by **5c** and **5h** by annexin V-FTTC/ PI assay

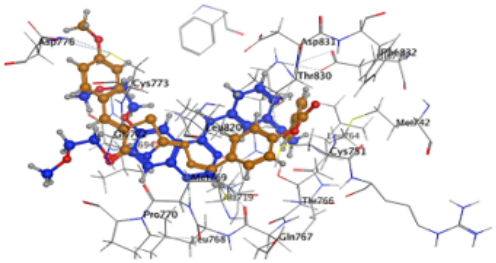

A

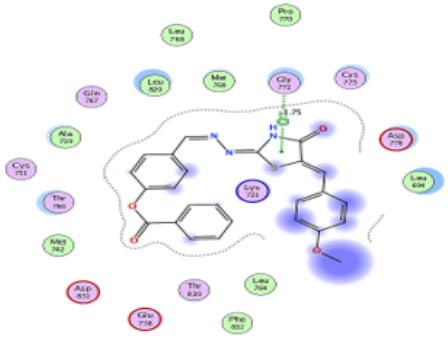

B

Figure 7

(**A**) Chart illustrated the 3D position between compound **5c** (orange) and the co-ligand erlotinib (blue) within the active site pocket of EGFR (PDB code 1M17) (**B**) Diagram illustrated the 2D binding of **5c** with the active site pocket of EGFR (PDB code 1M17) and the interaction with Gly 772

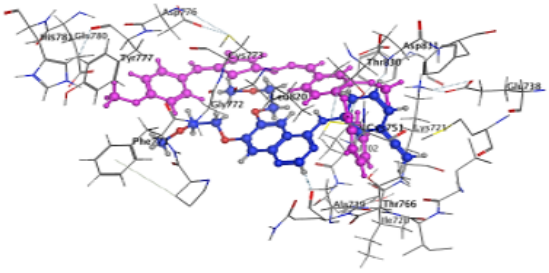

A

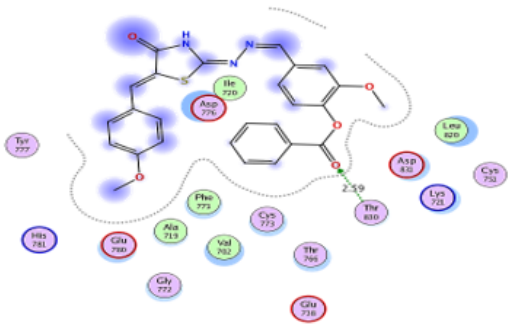

B

Figure 8

(A) Chart illustrated the 3D position between compound **5h** (purple) and the co-ligand erlotinib (blue) within the active site pocket of EGFR (PDB code 1M17) **(B)** Diagram illustrated the 2D binding of **5h** with the active site pocket of EGFR (PDB code 1M17) and the interaction with Thr 830

Supplementary Files

This is a list of supplementary files associated with this preprint. Click to download.

- supplimentryfile.docx
- Scheme1.png
- Scheme2.png
- Scheme3.png
- Scheme4.png
- Scheme5.png